Chapter 3
C-Mod Contributions to the FY2013 Joint Research Target

Amanda Hubbard[1], Dennis Whyte[1], John Canik[3], R. Michael Churchill[1], Istvan Cziegler[4], Arturo Dominguez[5], Martin Greenwald[1], Walter Guttenfelder[5], Nathan Howard[1], Jerry Hughes[1], Earl Marmar[1], Christian Theiler[1], Choongki Sung[1], Phil Snyder[2], John Walk[1], Anne White[1] and the Alcator C-Mod team

[1]*Plasma Science and Fusion Center, Massachusetts Institute of Technology*
[2]*General Atomics*
[3]*Oak Ridge National Laboratory*
[4]*Center for Momentum Transport and Flow Organization, Univ. California San Diego,*
[5]*Princeton Plasma Physics Laboratory*

1.0 Overview

This chapter of the FY2013 Joint Research Target report documents the contributions from the Alcator C-Mod team, including researchers at MIT and collaborators from other institutions. The Annual Target is:

> ***Annual Target***: *Conduct experiments and analysis on major fusion facilities, to evaluate stationary enhanced confinement regimes without large Edge Localized Modes (ELMs), and to improve understanding of the underlying physical mechanisms that allow acceptable edge particle transport while maintaining a strong thermal transport barrier. Mechanisms to be investigated can include intrinsic continuous edge plasma modes and externally applied 3D fields. Candidate regimes and techniques have been pioneered by each of the three major US facilities (C-Mod, D3D and NSTX). Coordinated experiments, measurements, and analysis will be carried out to assess and understand the operational space for the regimes. Exploiting the complementary parameters and tools of the devices, joint teams will aim to more closely approach key dimensionless parameters of ITER, and to identify correlations between edge fluctuations and transport. The role of rotation will be investigated. The research will strengthen the basis for extrapolation of stationary regimes which combine high energy confinement with good particle and impurity control, to ITER and other future fusion facilities for which avoidance of large ELMs is a critical issue.*

This report, and the research described in it, meet the requirements of the 4th Quarter Milestone, namely

> *Complete the required experiments and analysis. Prepare a joint report summarizing the contributions toward the development of high-performance stationary regimes devoid of large ELMs, and identifying important paths for future exploration.*

The target focusses on a crucial topic for fusion, since it is now clear that H-mode with Edge Localized Modes (ELMs), the standard high performance regime on most tokamaks, will have heat pulses which are unacceptable in ITER or a reactor. Active mitigation of ELMs, using magnetic perturbations or pellet injection, will be extremely challenging for ITER, and if it proves feasible will come at some penalty in confinement and fusion performance. Extrapolation of these techniques to a fusion reactor appears impractical, hence development of regimes with natural avoidance of ELMs is critical.

The Alcator C-Mod team has long been a leader in the development and study of quiescent, high performance, regimes. In fact, relatively few of its discharges have been in ELMy H-mode. The team pioneered the Enhanced D-alpha H-mode, in which increased particle transport and steady state are provided by an edge Quasicoherent Mode (QCM) [Greenwald 1999]. However, this regime is favored by relatively high collisionality and so may not extrapolate well to burning plasmas. Research in recent years has focused on the I-mode, also pioneered on Alcator C-Mod following early transient observations on both C-Mod and ASDEX Upgrade. This regime, described in the following section, combines several favorable characteristics: enhanced energy confinement with a strong thermal barrier near the last closed flux surface; little or no change in particle or impurity transport at the plasma edge, with L-mode like density profiles and global impurity confinement, hence no need for ELMs to regulate particle and impurity transport across the thermal barrier. Research for this milestone has focused on this regime, which as will be described appears to extrapolate well to the conditions of interest for fusion.

Since the Department of Energy did not fund operation of C-Mod in FY13, it has not been possible to do new experiments. However, analysis has been conducted of a large number of experiments conducted in FY12 and prior years. In particular, many discharges of the campaign in summer of 2012 were in the I-mode regime and had not been analysed at the start of FY13. Researchers from the Alcator C-Mod team also contributed strongly to the planning, execution and analysis of the DIII-D I-mode experiments described in Chapter 4.

This Chapter summarizes significant progress in the following areas:

- **Access conditions and operating space** (Section 2). A wide range of I-mode conditions have been achieved, closely approaching many key dimensionless and dimensional parameters of ITER.
- **Pedestal structure and stability** (Section 3). Detailed profile measurements and macrostability analysis explain the typical lack of ELMs in terms of distance from stability limits, and show key and favorable differences in pedestal width and height scaling from ELMy H-mode. Microstability analysis of the I-mode pedestal is beginning.
- **Turbulent fluctuations and role in transport** (Section 4). Density, temperature and velocity fluctuations have been analysed and new results shed light on the changes in, and separation of, particle and energy transport. Decreases in pedestal and core broadband turbulence correlate with reduced thermal transport in I-mode. A Weakly Coherent Mode usually observed in the pedestal region is linked to particle transport, and interacts with a newly identified

fluctuating zonal flow (Geodesic Acoustic Mode) which may play a key role in the regime and in transitions.

Finally Section 5 describes some of the many opportunities for further progress in this research which could be accomplished with continuing support of experiments on, and analysis of results from, Alcator C-Mod.

1.1: Description of the C-Mod I-mode regime and key prior results.

The key defining feature of the I-mode regime is the appearance of an edge *thermal* transport barrier, leading to pedestals in electron and ion temperature, without an accompanying *particle* transport barrier, hence L-mode like density pedestals and impurity transport. An example, presented at the 2010 IAEA Fusion Energy Conference [Whyte 2010], is shown in Figure 3.1-1.

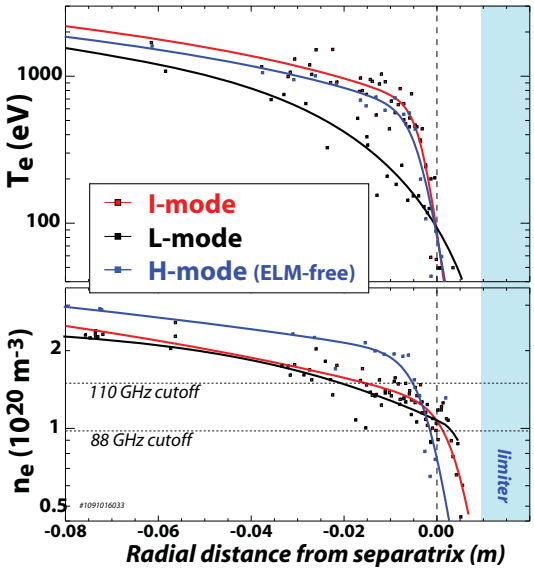

Figure 3.1-1: Examples of radial profiles from the outer third of the plasma for L-mode, I-mode and ELM-free H-mode phases of a C-Mod discharge (upper single-null, B_T = 5.6T, q_{95} ~ 3.2). Profiles are fitted to a modified tanh function. Slices are shown in (a) electron temperature from TS and ECE (b) electron density from TS. From [Whyte 2010]

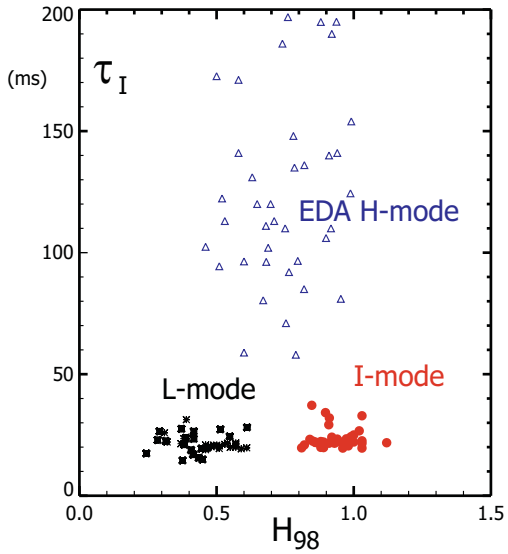

Figure 3.1-2: Measurements of particle confinement of injected Ca impurities vs. normalized energy confinement, for representative C-Mod L-mode, I-mode and EDA H-mode discharges. I-modes (red) have H-mode τ_E but L-mode τ_I.

These differences in edge particle and thermal transport are reflected in the global confinement properties. Figure 3.1-2 plots the impurity confinement time τ_I, measured using injection of Ca, and the energy confinement normalized by the

ITER98y2 scaling for H-modes [ITER 1999]. $H_{98,y2}$ reaches levels typical of H-modes, while τ_I remains at L-mode levels (20-30 ms) [Howard 2011]. Even the 'low particle confinement' EDA H-modes have τ_I up to 10 times higher, while standard "ELM-free" H-modes, such as the blue profile in Figure 3.1-1, have τ_I exceeding the pulse length of ~1 sec. ELM-free H-modes are thus intrinsically transient, with electron and impurity densities steadily rising and cooling the discharge; while confinement can be high they do not meet the requirements of stationarity which are the focus of this Joint Research Target. In contrast, I-mode has been developed by the C-Mod team into a highly robust, stationary, high performance regime.

An example discharge from the 2012 campaign is shown in Figure 3.1-3. The global energy confinement exceeds the ITER98y2 scaling. Errors bars on H_{98} represent the uncertainty in estimating fast particle contributions to the stored energy. There is no increase in density or radiated power after transition to I-mode. Safety factor q_{95} is 3.4; other examples have q_{95} below 3, spanning the planned range on ITER. Even at the maximum power available, nearly 5 MW of ICRH, there is no transition to H-mode; the I-mode phase continues until the heating is reduced.

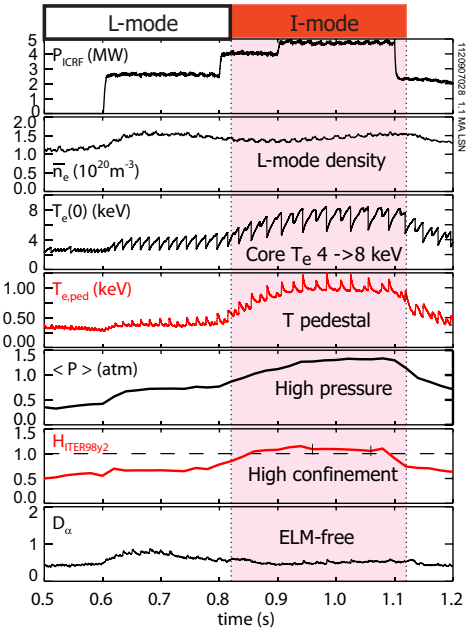

Figure 3.1-3: Time evolution of C-Mod discharge 1120907028 (5.8 T, 1.1 MA). I-mode is maintained up to the maximum ICRF power of 4.8 MW, with T_e (0) 8 keV, T_{ped} 1 keV and confinement at the H_{98y2} level.

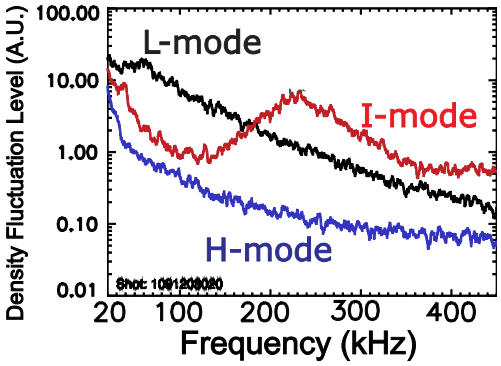

Figure 3.1-4: Reflectometer fluctuations (88 GHz, n_c= 9.6 x10^{19} m^{-3} (r_c/a ≅ 0.95) for a typical q_{95}=3.1 C-Mod discharge 109120320 (1.3 MA, 5.8 T, upper single null). Spectra are averaged over 20 ms, in L-mode (black), I-mode (red) and H-mode (blue).

Historically, modest increases in edge temperature and confinement were observed, usually transiently, in discharges with ion **B**×∇B drift away from the active x-point, which is known to increase the H-mode power threshold [Greenwald 1997, Ryter 1998, Groebner 1998, Carlstrom 1998]. This phenomenon was termed 'improved L-mode' on ASDEX Upgrade [Ryter 1998]. It was shown on C-Mod that due to profile stiffness, global confinement also improved. As edge profile and fluctuation diagnostics improved, it was noted that changes in broadband fluctuation spectra accompanied the reduction in edge transport, with decreases at moderate f and increases at f > 150 kHz [Hubbard 2007].

From the 2009 operating campaigns, the regime was progressively extended to long duration and high confinement, and its potential for an attractive fusion regime was recognized. It was renamed "I-mode", since L-mode seemed a misnomer given the high confinement [McDermott 2009]. Improved fluctuation and profile diagnostics showed the typical presence of clear signatures – a decrease in broadband turbulence in the 50-150 kHz range when the T pedestal formed, along with a clear E_r well. At the same time a peak in fluctuations at typically 200-400 kHz is generally observed. This was named the 'Weakly Coherent Mode' (WCM) due to its broad spectrum, with $\Delta f/f \sim 0.3\text{-}1$. Representative spectra in each regime are shown in Figure 3.1-4. In the I-mode phase (red), mid-f turbulence decreases to levels near H-mode, while the peak of the 'weakly coherent mode' exceeds the L-mode level [Hubbard 2011].

The WCM has now been observed in electron temperature fluctuations as well as in density and magnetic turbulence (Figure 3.1-5) [White 2011]. The relative level of turbulent fluctuations is lower (1-1.6%) in T_e than in n_e (6-13%). All fluctuations are localized to the region of the T_e and T_i pedestal. Details of these fluctuations are presented in Section 4.2.

The I-mode regime is most often obtained in the unfavorable drift configuration, with ion **B**×∇B drift away from the active x-point. For C-Mod this can be achieved either by reversing the magnetic field and current for discharges with dominant x-points near the closed lower divertor, or in 'normal' field with an x-point near the open upper divertor. The power threshold for L-I transitions generally exceeds L-H scalings developed for favorable drift, and has somewhat different scaling [Hubbard 2012]. Access conditions are discussed further in the following section. Experiments in 2010 demonstrated that I-mode can be also robustly accessed in specific LSN shapes with *favorable* drift, and be extended to steady state (> 10 τ_E). In this case thresholds are near L-H scaling laws, and much lower [Hubbard 2011]. While normalized confinement remains at H-mode levels, the power range is small and absolute performance is thus modest. This report thus focusses on results obtained with the unfavorable drift configuration.

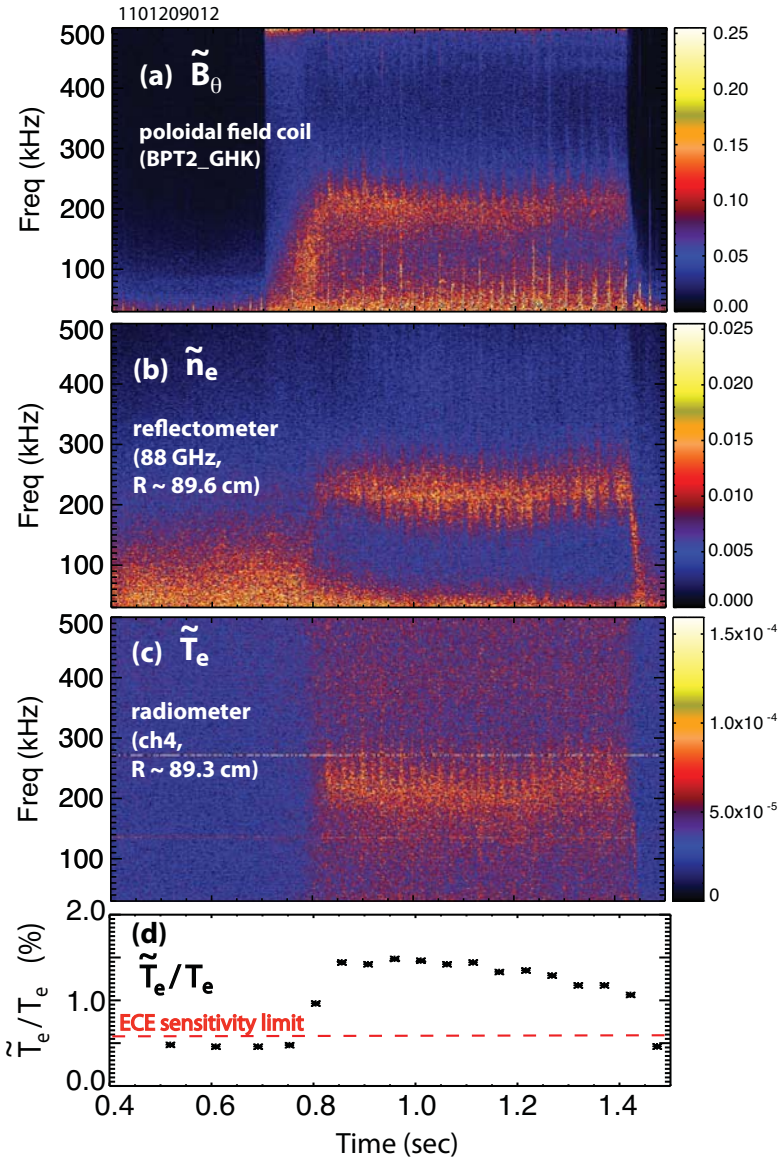

Figure 3.1-5: Contours of time-resolved spectra from edge fluctuations showing typical WCM features during I-mode (0.8 < t < 1.5). (a) Autopower spectrum of an edge poloidal magnetic field probe. (b) Autopower spectrum of an edge reflectometer signal ($f_{o\text{-}mode}$ = 88 GHz, R = 89.6 cm). (c) Autopower spectrum of edge ECE radiometer channel (f_{ece} = 241.8 GHz, R = 89.3 cm). (d) Temperature fluctuation level, $\delta T_e/T_e$(%), in time, calculated from the radiometer channel. The sensitivity limit is shown as the red dashed line. From [White 2011]

2.0 Access and operating space of I-mode regime

2.1: Parameter space of C-Mod I-modes

The I-mode regime on C-Mod has proven remarkably robust, over extremely wide ranges of operating parameters, encouraging for its extrapolation to other devices. Over 260 discharges and time slices have been analysed and added to databases, with still more remaining to be added. These represent a wide range of plasma parameters, B_T=3.0-6.1 T, I_p=0.8-1.35 MA, q_{95}=2.5-5.3, loss power $P_{loss} \equiv P_{ohmic} + P_{RF,abs} - dW/dt$ =1.6-5.1 MW and average density $\bar{n}_e$=0.85-2.3x10^{20} m^{-3}. The field, q_{95} and density ranges span those of ITER and there is no apparent physics barrier to accessing the regime. Figure 3.2-1 shows the ranges of field and current in the scalar database, and in a newly created database of pedestal profiles, described in Section 3. In particular, I-modes extend to, and have highest performance in, low collisionality and q_{95}, both important for ITER. (Figure 3.2-2) This contrasts with the EDA H-mode which generally occurs at $\nu^* > 1$ and $q_{95} > 3.5$ [Greenwald 1997].

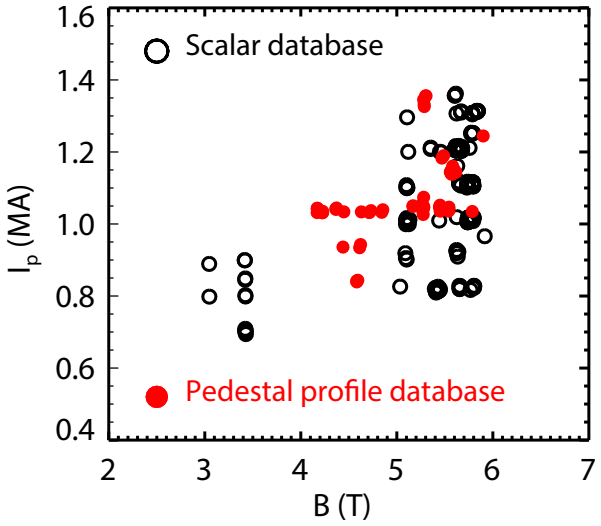

Figure 3.2-1: Ranges of plasma current and toroidal field in C-Mod I-modes covered by a database of scalar parameters (black), which has been extended during FY13 and a newly created database containing detailed pedestal fits (red).

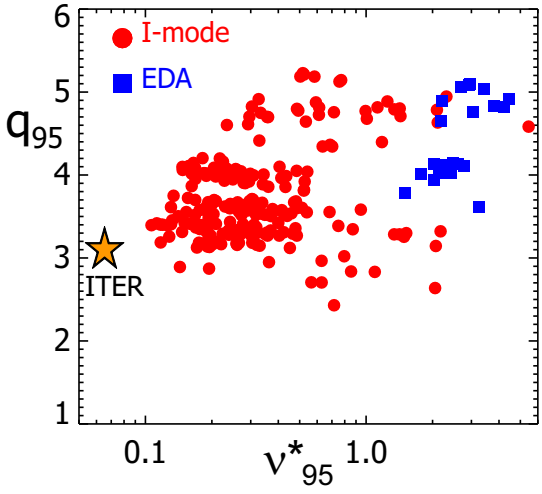

Figure 3.2-2: Range of safety factor q_{95} vs collisionality ν^* in C-Mod I-modes. A few representative discharges in the EDA H-mode regime are shown for comparison.

Regions of configuration and parameter space have been identified in which I-mode is robustly accessed at moderate input power, and can be sustained at powers up to the maximum available (5 MW ICRF heating, a large power density for a device with 1.1 m^3 plasma volume). Stationary I-modes are now routinely sustained for the duration of the plasma discharge and heating power pulse, many energy and particle confinement times.

The optimal configuration to date uses reversed field and current, with upward ion B×∇B drift and the X-point towards the closed lower divertor, and moderate L-mode target densities, typically in the range $\bar{n}_e$=1.0-1.5x10^{20}m^{-3}. An example was shown in Figure 3.1-3.

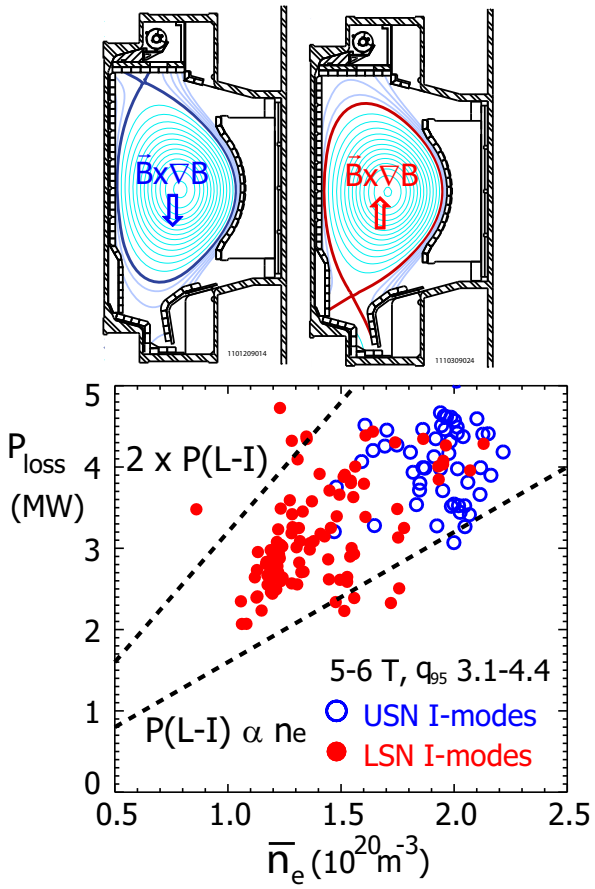

*Figure 3.2-3: Loss power vs. $\bar{n}_e$ for a subset of I-mode discharges with B_T 5-6 T and q_{95}=3.1-4.4, comparing two configurations with unfavorable ion **B**×∇B drift. The LSN, reversed B_T configuration (closed red points) has a wider density and power range.*

Figure 3.2-3 compares the operating space achieved to date for a restricted current and field range, in the upper null, forward field (blue) and lower null, reversed field (red) configurations. The LSN I-modes extend to lower density, and have a wide power range at these reduced densities, robustly maintained with at least twice the power required to access the regime, and up to the maximum heating power available (5 MW ICRF). Higher powers are likely possible; transitions to H-mode are

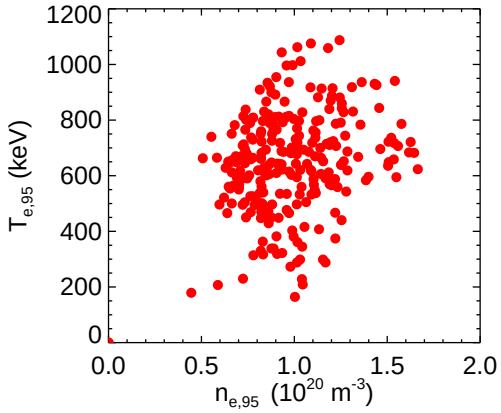

Figure 3.2-4: Temperature vs. n_e at ψ=0.95 for all C-Mod I-modes in the scalar database.

rare in these conditions. The reason for the difference between LSN and USN I-modes is not clear, but may be related to slight differences in shape, or to the interactions of the separatrix and SOL with the closed lower divertor. Due to high SOL power densities, a limited range of shapes is possible in each configuration. Impurity seeding, usually with Neon, is used in some cases to reduce heat fluxes, and due to the low impurity confinement characteristic of I-mode is found to be compatible with high performance.

The C-Mod I-mode dataset also covers a very wide range of edge parameters. Density and electron temperature at the 95% flux surface are shown in Figure 3.2-4.

2.2: Thresholds and power range

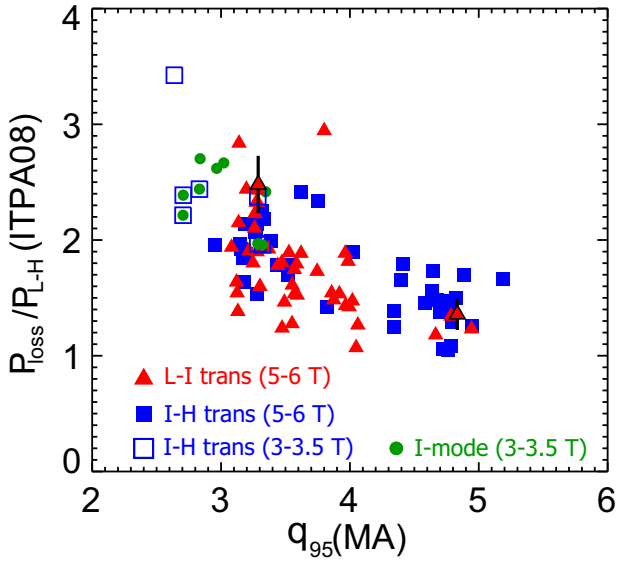

Figure 3.2-5: Threshold power for L-I transitions (red triangles) and I-H transitions (blue squares) in unfavorable drift, normalized to the ITPA08 scaling for L-H transitions with favorable drift. I-mode thresholds are higher and have a q_{95} dependence not present in the L-H scaling.

There has been extensive study of the conditions for accessing I-mode on C-Mod, and for remaining in the regime before I-H transitions. Scalings for the L-I transition were developed in 2012 and have since been extended with more experiments. Comparison of power thresholds with the ITPA scaling $P_{Thres,ITPA08} = 0.0488\ n_{e20}^{0.717}\ B_T^{0.80}\ S^{0.941}$ [Martin 2008] for L-H transitions in favorable drift is shown in Figure 3.2-5. The L-I threshold is 1-3 times higher, and has a q_{95} dependence not in the L-H scaling. The 2012 regression analysis of the data set of L-I transitions was restricted to discharges with B_T= 5-6 T which had widest variation of current and density. The best fit was $P_{thresh}=2.11\ I_p^{0.94\pm0.24}\ \bar{n}_e^{0.65\pm0.18}$, confirming a strong current dependence as suggested by the normalized scaling above [Hubbard 2012].

Attempts to scale the I-H threshold have been less successful; there is a great deal of scatter even for fairly comparable conditions, in both power and local parameters. As noted above, the widest power range, at least a factor of two, is found in LSN, reversed B_T discharges with relatively low density. The density range in this configuration was extended to both higher and lower density in 2012 experiments. Fig 3.2-6 shows results from a dedicated experiment carried out in August and September 2012, with fixed LSN shape, field and current (5.8 T, 1.1 MA, q_{95}=3.5). These show for the first time the existence of a minimum in the P_{L-I} vs n_e dependence; power thresholds (green triangles) increase roughly linearly above about 1.3 x 10^{20} m^{-3}, but also increase at lower density. The lowest density for which I-mode was achieved was 0.89 x 10^{20} m^{-3}.

The upper limit of density for given parameters and configuration has in the past been set by the range for which L-I transitions occurred; above a certain density (1.8 x 10^{20} m^{-3} in the conditions of Figure 3.2-6), transitions directly from L to H-mode occur. In general the power range between L-I and I-H thresholds (blue squares) becomes narrow at higher density. This has been a potential concern for extrapolation to burning plasmas; while lower density is advantageous for accessing I-mode with moderate power, higher densities are optimal for fusion performance. It is thus desirable to increase density during the I-mode phase.

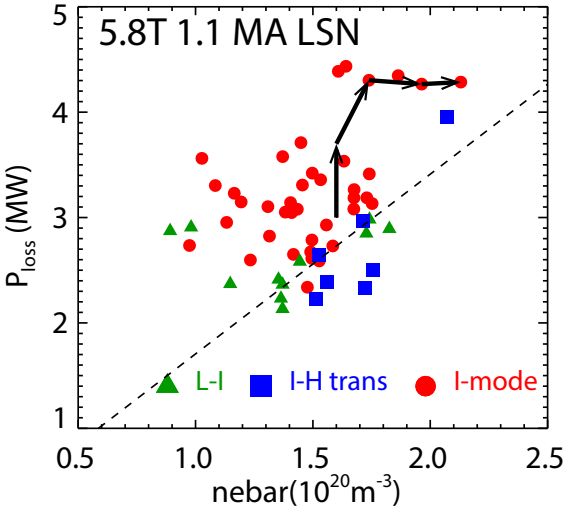

Figure 3.2-6: Loss power vs. line averaged density for an experiment with fixed conditions. This shows a minimum in the power threshold for L-I transitions (green triangles, and an upper limit to the density at which transitions to I-mode occurred. However, higher density could be achieved by fuelling into I-modes; the arrows show the time trajectory of the discharge in Fig. 3.2-7.

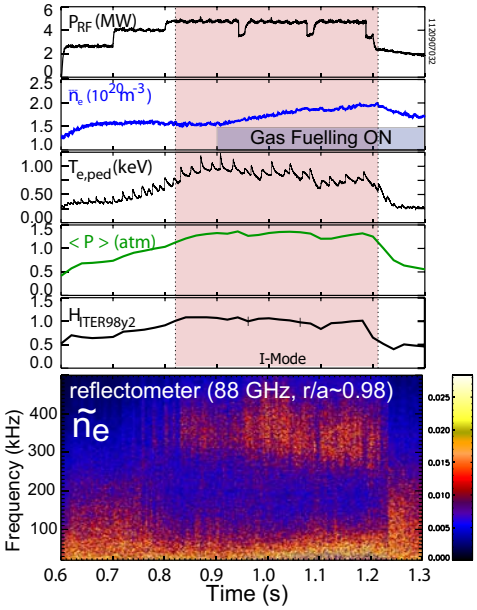

Figure 3.2-7: Time traces and edge density fluctuations for a discharge similar to that shown in Fig. 3.1-3 but with gas fuelling during I-mode. Density is increased 30% while maintaining core pressure and confinement.

Initial C-Mod experiments are quite encouraging in this regard. Gas fuelling was added to an I-mode phase similar to that of Figure 3.1-3, increasing $\bar{n}_e$ from 1.5 to 2 x $10^{20}$$m^{-3}$ (Fig. 3.2-7). Stored energy remained nearly constant, with $H_{98y2} \geq 1$, and I-mode turbulence features and transport barrier are clearly maintained. The trajectory of this discharge is shown on Fig. 3.2-6, and shows that I-mode is maintained for powers well above that which resulted in I-H transitions when starting from higher target density. In a subsequent discharge, an I-H transition resulted from a *decrease* in heating power at comparable density (top right blue square). This suggests that maintaining an edge T_e gradient is important in driving the higher frequency turbulence which appears to drive

particle transport, and to avoid H-mode transitions. Thus, with further increases in power, from external sources or from alphas in a burning plasma, it could well be possible to extend the I-mode operating space to even higher densities and performance. In short, the limits of I-mode operating space on C-Mod have by no means been reached, and further experiments are highly desirable to assess the ultimate potential of the regime.

2.3: Global confinement and performance

Importantly, good global confinement is maintained across the wide parameter space of I-modes. Figure 3.2-8 shows H_{ITER89} vs q_{95}; levels exceeding the H-mode scaling which is the basis for ITER performance projections are achieved down to q_{95} below 3, the ITER H-mode operating point. H_{ITER89} ranges from 0.7 to 1.2. Stored energy is calculated from magnetics, so that there

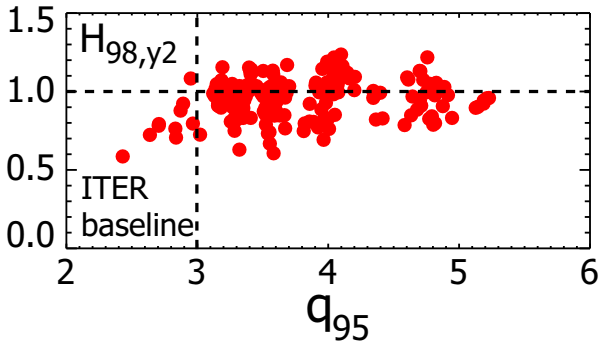

Figure 3.2-8: Normalized confinement $H_{98,y2}$ vs q_{95} in I-modes. The C-Mod discharges meet the requirements of the ITER baseline scenario in both parameters.

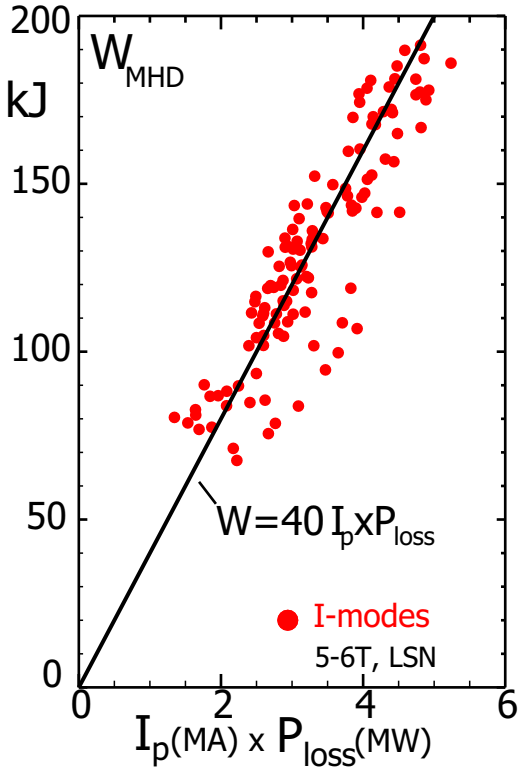

Fig 3.2-9: Stored energy vs I_p P_{loss} in lower single null I-modes. In contrast to H-modes, W scales linearly with power.

may be some contribution from fast particles in the highest temperature cases. A key and very positive difference between I-mode and H-mode confinement scaling is the much weaker, perhaps no, degradation with input power. The stored energy increases close to linearly with power, as shown in Figure 3.2-9. In contrast, the H-mode confinement scaling $\tau_{ITER\text{-}H98,Y2}$ decreases strongly with power, as $P^{-0.69}$. This means that for given global parameters, the normalized confinement generally increases with input power. The very favorable I-mode scaling likely reflects the fact that the boundary is away from stability limits. The height of the temperature and pressure barrier also scales approximately linearly with increasing heating power, unlike H-modes where it tends to saturate. Detailed measurements and analysis of the critical pedestal region are presented in the following section.

3.0 Pedestal and stability analysis

3.1: Pedestal structure

The structure and stability of the pedestal region in I-mode is key to understanding both its favorable transport properties and its general lack of large ELMs. A major emphasis of efforts in 2013 has been to analyse profiles in this region, from the extensive set of FY2012 experiments, using upgraded diagnostics and analysis techniques. These use data from a suite of high resolution diagnostics, including Edge Thomson Scattering (ETS) for n_e and T_e, and CXRS on both the high and low field side for ion profiles and flows, from which E_r profiles are being derived [Churchill 2013a]. An extensive recalibration of the ETS diagnostic was performed during the C-Mod shutdown. This has resulted in more accurate profiles, and revealed that T_e pedestals can be even higher than was previously thought. T_e profiles can be substantially modified by sawtooth heat pulses, necessitating carefully synchronized averaging. An example of electron profiles from the stationary high performance I-mode discharge of Figure 3.1-3 is shown in Figure 3.3-1.

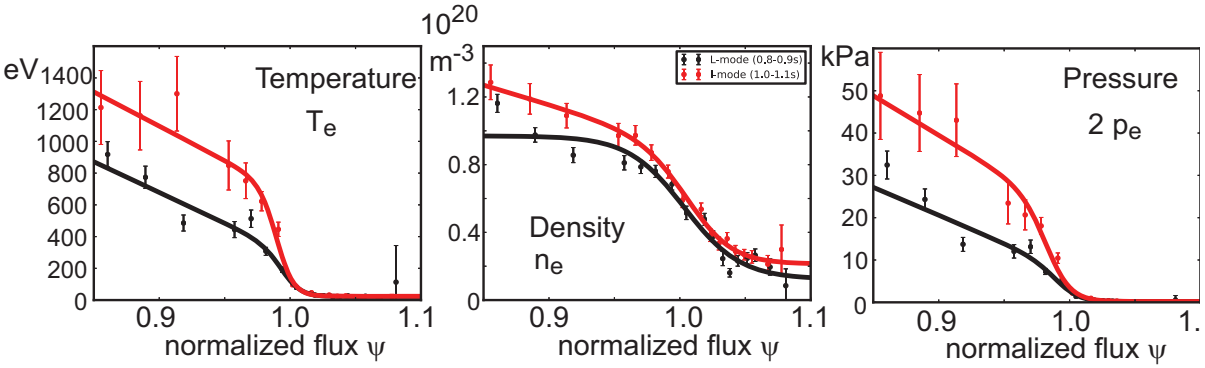

Figure 3.3-1: Electron pedestal profiles from an I-mode (red) vs L-mode (black) phase of a C-Mod discharge. The temperature exhibits a strong pedestal in I-mode, while the density structure is nearly identical to L-mode. The pedestal pressure and gradient are also higher in I-mode.

A new data set of global parameters and tanh fit parameters from such carefully analysed profiles has been created. It currently contains 72 time slices from a wide range of plasma parameters including dedicated scans in FY2012 (0.84-1.35MA current scan, 4.34-6.1T field scan, 1.0-1.9 scan in average density (equivalent to a Greenwald fraction scan of 0.13-0.25). Preliminary results from a smaller dataset were presented at the 2013 TTF meeting and included in the second quarter JRT report. The fitted profiles allow pedestals in I-mode to be compared with those previously studied, and simulated with models, in ELMy and EDA H-modes [Walk 2012, Hughes 2013].

The ELMy H-mode studies have shown that the pressure pedestal is well predicted by the EPED model [Synder 2009], in which the pressure limit is set by a combination of peeling-ballooning modes and kinetic ballooning modes. The pedestal width scales with the square root of pedestal poloidal beta β_{pol}, as shown in Figure 3.3-2. This is consistent with results from several other tokamaks. Together, this validation has resulted in a prediction for ITER [Groebner 2013, Hughes 2013]. In contrast, pedestals in I-mode are significantly wider than H-modes of comparable β_{pol}, up to 5% in normalized flux. As shown in the same figure, they do not show any scaling trend with β_{pol}. This is consistent with gradients being below kinetic ballooning limits, suggesting that a different physical mechanism regulates the pedestal. The broader pedestal gives the potential to further increase pedestal heights without violating MHD limits. Stability analysis is presented in the following section.

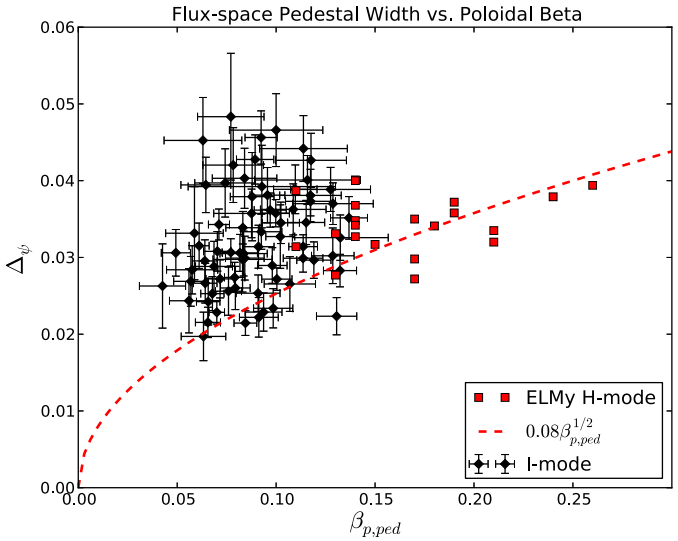

Figure 3.3-2: Measurements of pressure pedestal widths vs poloidal beta. ELMy H-modes follow the scaling predicted by the EPED model [ref], while I-mode pedestals are typically wider for comparable β_P.

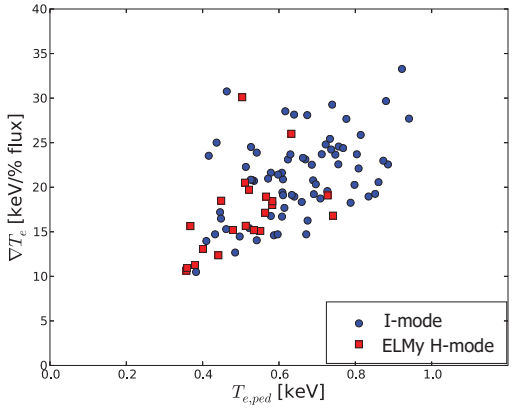

Figure 3.3-3: Electron temperature gradient vs pedestal height, for sets of I-modes (blue circles) and ELMy H-modes (red).

Analysis of trends in I-mode pedestal height, width and gradients is in progress. An example is shown in Figure 3.3-3, which compares the height and gradient of T_e pedestals with those in ELMy H-mode. While there is considerable overlap, the I-mode plasmas extend to hotter and steeper pedestals. This work will be presented by MIT graduate student John Walk in an invited talk at the APS-DPP meeting in November, 2013.

Charge Exchange Recombination Spectroscopy (CXRS) diagnostics, viewing both the high and low field side of C-Mod, are used to measure for ion profiles and flows. An ion temperature pedestal develops which is, within experimental uncertainties, equal to that in T_e. Toroidal rotation in the co-current direction also increases. This is correlated to temperature gradient; comparing rotation in I-mode and H-mode has been important in understanding the source of this intrinsic rotation [Rice 2011]. From these, E_r profiles are being derived. Steep E_r wells are observed in I-mode, in the region of the temperature pedestal, as shown in Figure 3.3-4. Both the diamagnetic and the poloidal flow term in the radial impurity force balance equation contribute significantly to E_r. Strong gradients in the poloidal flow, just inside the LCFS, make the E_r well asymmetric with a strong shear layer on its outer side. Besides an approximately 20% wider E_r well, this asymmetric structure is the main difference compared to E_r of EDA H-modes. Careful in-vessel calibrations have been performed to spatially align CXRS measurements with fluctuation measurements from GPI such that the location of the Weakly Coherent Mode inside the E_r well can be determined and the effect of the E_r shear on the WCM be investigated. Efforts to achieve this are still ongoing and possibly require a deconvolution of the measured profiles from instrumental effects. This has so far only been performed for the CXRS system. Measurements of boron density show an in-out asymmetry in the H-mode regime, but not in either I-mode or L-mode [Churchill 2013b]. This is again consistent with L-mode-like particle transport in the I-mode regime.

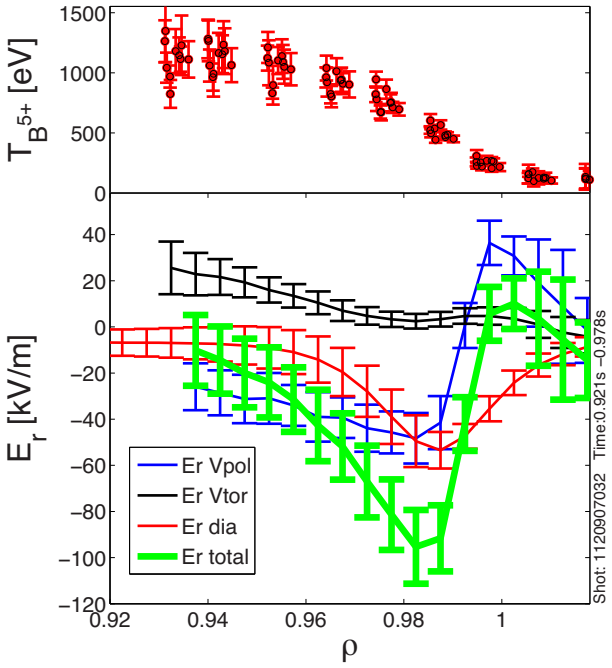

Figure 3.3-4: Profiles of boron temperature (top) and E_r components in a high power I-mode discharge, from CXRS.

3.2: Pedestal stability

The accurate pedestal profiles now available, in high performance I-modes, have enabled analysis of the MHD stability in the plasma region. This is important in understanding the avoidance of ELMs, one of the most important features of the regime, and in assessing the potential for further increases in pedestal pressure and global performance.

The theory of peeling-ballooning modes has been highly successful at explaining the onset conditions for Type I ELMs on a number of tokamaks, particularly through its model implementation in the ELITE code [Wilson 2002]. ELITE was used previously to test the peeling-ballooning stability of several EDA H-mode discharges, some of which exhibited small, irregular ELMs in addition to the usual QCM [Mossessian 2003]. In these cases, calculated stability to peeling-ballooning modes was indeed correlated with the absence of ELMs. More recent calculations take advantage of a technique to perturb the pressure gradient and current profile about the experimental reconstruction, and evaluate stability on a grid of $(p', j_{||})$. This technique yields contours of $\gamma_{max}/\omega_{eff}$, the maximum linear growth rate normalized to a stabilization rate. Here, $\gamma_{max}/(\omega_{eff}/2)<1$ is the criterion for stability where ω_{eff} is derived from earlier calculations done with the BOUT++ code [Dudson 2009], which gave a quantitative description of diamagnetic stabilization of ideal peeling-ballooning modes at moderate to high n-number [Snyder 2012].

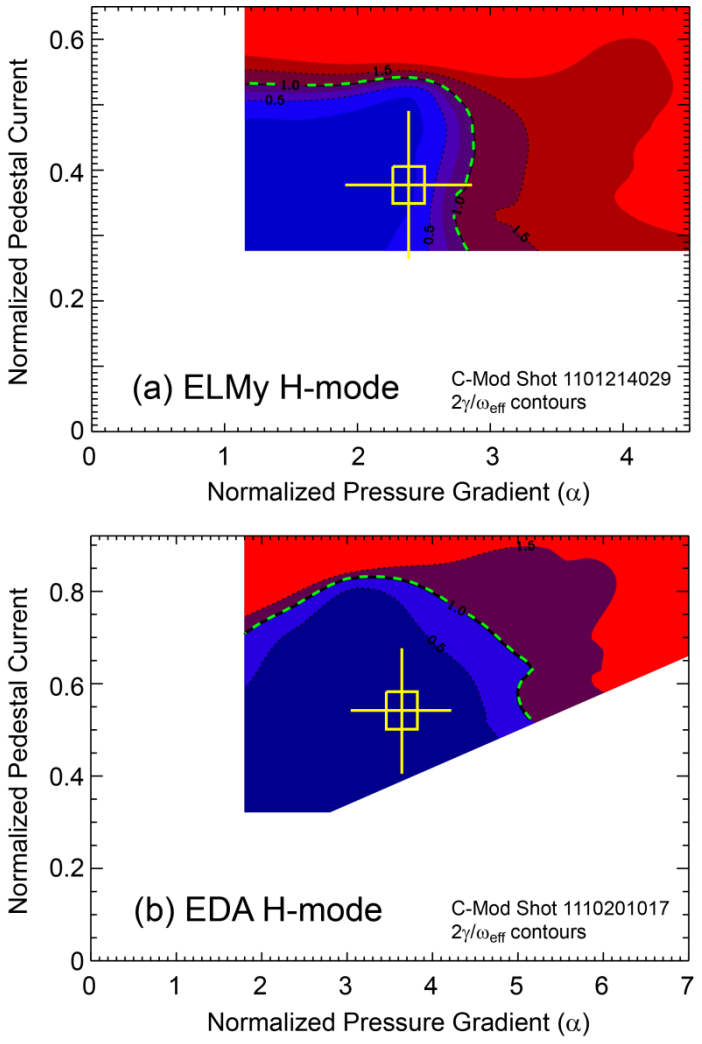

Figure 3.3-5: Peeling-ballooning stability calculated with ELITE in (a) ELMy H-mode and (b) EDA H-mode, with experimental points marked by cross-hairs [Hughes 2013].

Discharges with ELMy H-modes in C-Mod, analysed using the ELITE code, do indeed lie near the predicted stability boundary, consistent with the peeling-ballooning model. An example is shown in Figure 3.3-5(a) [Hughes 2013]. Within experimental uncertainties, the pedestal is at the calculated stability boundary, with the most unstable modes occurring at moderate n, and near the pressure-limited side of the stability contour.

Pedestals in the quiescent EDA H-mode regime, which in common with I-mode do not exhibit large ELMs, tend to exist farther in phase space from the contour of instability. This is illustrated in Fig. 3.3-5(b).

In comparison to ELMy H-modes, I-modes generally have comparable or higher temperature pedestals but much weaker density gradients, as illustrated in Figure 3.3-6 (a,b). Also, as noted above the pedestals tend to be wider. There is thus substantial reduction in pressure gradient and bootstrap current drive, relative to H-mode, making I-modes quite stable to peeling-ballooning modes. These profile differences are also evident in Figure 3.3-6(c,d).

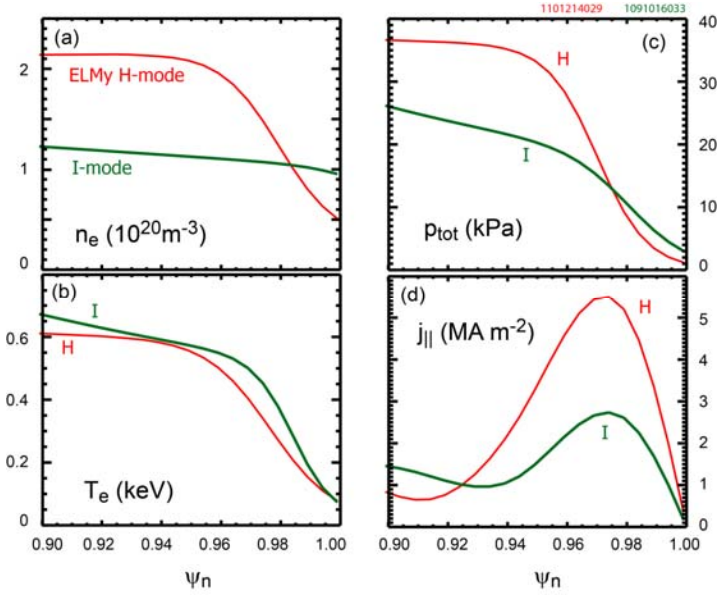

Figure 3.3-6: Model profiles, fitted from experimental data, used as inputs to MHD stability analysis of ELMy H-mode (red) and I-mode (green). Shown are (a—b) electron density and temperature, (c) total pressure, and (d) low-field side current density, all as a function of normalized poloidal flux [Hughes 2013].

For the I-mode shown, ELITE calculations find growth rates an order of magnitude or more below the instability criterion. Because I-modes of modest performance, such as this example, operate so far from the stability boundary, this boundary can be challenging to find with the perturbative technique outlined above. However, indications are that the boundary is very similar to that in an H-mode of similar pedestal pressure and thermal stored energy. As seen in Fig. 3.3-7, substantial increases in pedestal p′ are possible within the constraints of the peeling-ballooning limit, allowing for considerable increases in performance while still remaining ELM-suppressed.

Recently, stability analysis was performed for a higher performance I-mode discharge 1120913026. In this case the peeling-ballooning boundary was reliably determined. Preliminary results, shown in Figure 3.3-8, indicate that the experimental conditions were again well away from this boundary, consistent with the lack of ELMs and indicating that further increases in the pedestal are possible. The solid line shows stability contours for infinite-n ballooning MHD modes calculated by BALOO [Connor 1979], which are used

as an indication of the KBM threshold. They indicate that the pedestal is also stable to KBMs, consistent with the width scaling in Figure 3.3-2. This MHD stability analysis has been carried out as part of the thesis work of an MIT graduate student, in collaboration with Phil Synder of General Atomics.

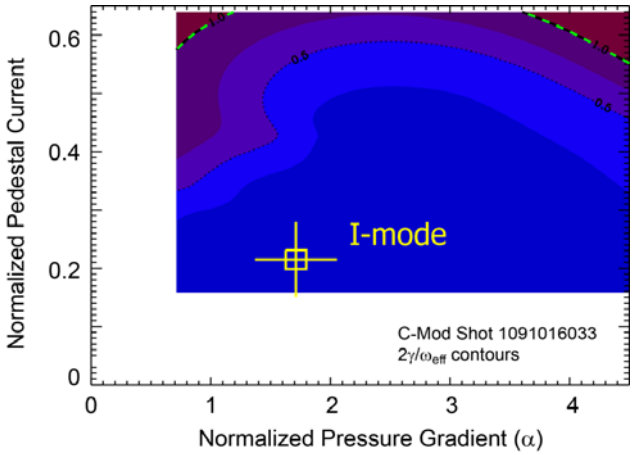

Figure 3.3-7: I-mode operating point (cross-hairs), and approximate boundary for peeling-ballooning stability (dashed curve), for the moderate performance discharge whose profiles are shown in Figure 3.3-6.

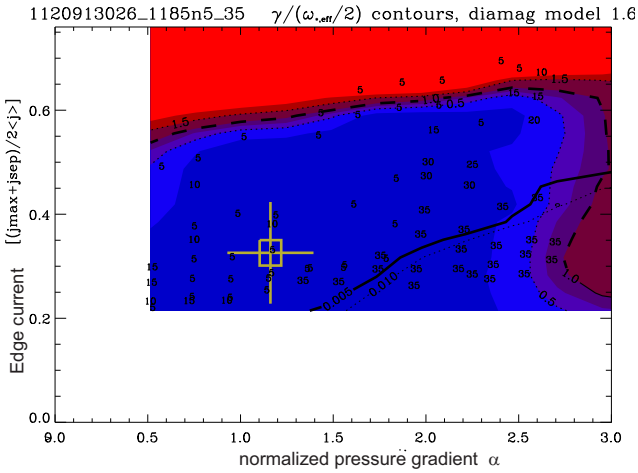

Figure 3.3-8: I-mode operating point (cross-hairs), and approximate boundary for peeling-ballooning stability (dashed curve), for a higher performance I-mode discharge with I_p 1 MA, B_T 4.8 T, 3 MW ICRH, which reached central T_e 6 keV.

Given the macrostability of the I-mode pedestal, and lack of ELMs, other mechanisms, as yet uncertain, appear to be regulating the transport and maintaining steady conditions. Microstability analysis has begun in FY13 to identify the potential sources of observed fluctuations, which are discussed in the following section. Linear gyrokinetic calculations using GS2 and GYRO (J. Canik [ORNL], W. Guttenfelder [PPPL]) have been performed for both the H-mode and I-mode cases, beginning just inside the steep gradient region (e.g. at ψ_N~0.94) and steadily progressing outward (e.g. toward ψ_N =0.98). Very good agreement in both real and imaginary parts of growth rates has been obtained in the code-to-code comparisons, shown in Figure 3.3-9, with agreement becoming somewhat poorer as collisions are implemented in the calculations. Promising signatures exist in the code results which might have a link to the WCM that is experimentally observed in I-mode.

Specifically, in the range of k_θ that is associated with the WCM fluctuation, linear unstable modes are found with real frequencies of tens of kHz, and propagating in the electron diamagnetic direction. Future plans for this analysis, using the high performance I-mode data sets with improved edge Thomson and CXRS data shown above are to: (a) push calculations farther into the steep gradient region, (b) establish sensitivity of results

to highly variable experimental quantities such as the gradient scale length of the temperature pedestal, and (c) examine the ratio of quasi-linear heat and particle fluxes and compare with H-mode.

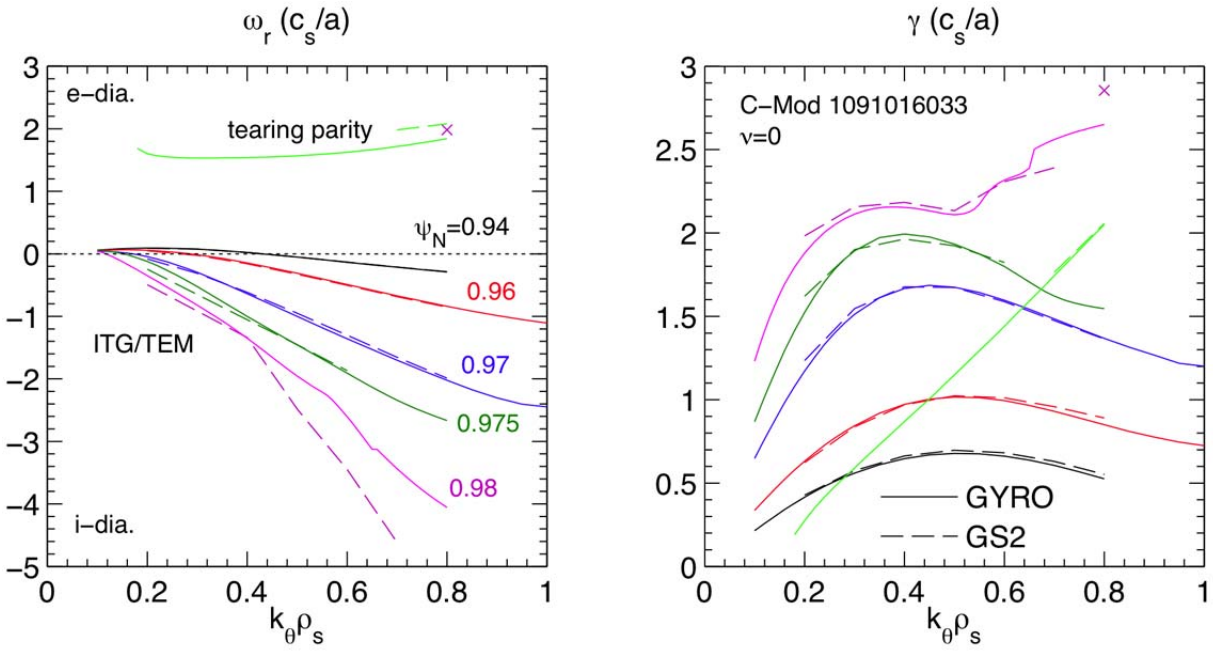

Figure 3.3-9: Initial linear gyrokinetic simulations of the pedestal in a C-Mod I-mode discharge, for various normalized radii. Collisionless simulations with GS2 (dashed curves) and GYRO (solid) agree very well.

4.0 Turbulent fluctuations and their role in transport

4.1: Pedestal broadband turbulence and its role in energy transport

Considerable progress has been made in characterizing the edge and SOL turbulence, transport and profiles, and the relationships between them. A key signature of the L-I transition, accompanying the formation of T_e and T_i pedestals, is the reduction of edge broadband turbulence in intermediate frequencies, typically ~60-150 kHz. This contrasts with the usual increase in such turbulence with increased heating in L-mode. The reduction is seen most clearly in density, on reflectometry channels located in the outer 5-10% of the plasma, and is also visible in magnetic fluctuations. A good correlation in time has been observed between the level of density fluctuations and the reduced thermal conductivity χ_{eff} inferred from power balance analysis in the outer 5% of the plasma, as shown in Figure 3.4-1 [Hubbard 2011]. This suggests that turbulence in this frequency range is an important contributor to thermal transport. The reduction may be related to the development of an E_r well in I-mode, which as shown in Section 3.1 is clearly evident from CXRS diagnostics though weaker than in H-modes [McDermott 2009]. It has been observed, to varying degrees, in all I-mode phases on C-Mod.

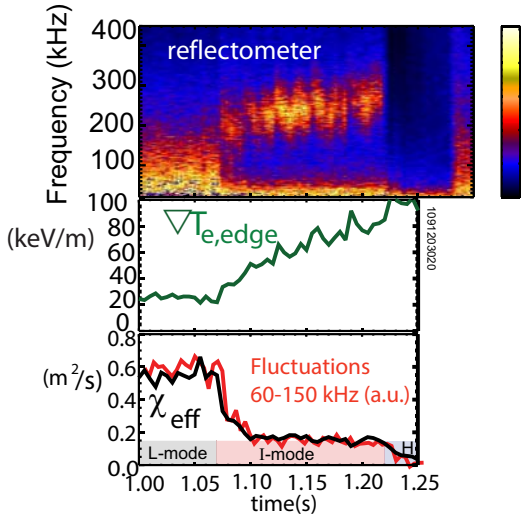

Figure 3.4-1: Reflectometer fluctuations at $n_c = 9.6x10^{19}m^{-3}$ ($r_c/a \cong 0.95$) and edge thermal transport in L, I and H-mode for a $q_{95}=3.1$ C-Mod discharge 109120320 (1.3 MA, 5.8 T, upper single null). The decrease in fluctuations integrated over the 60-150 kHz frequency band (red trace) correlates with the computed χ_{eff}, decreasing from L-mode to I-mode, and further in an ELM-free H-mode.

4.2: Weakly coherent mode and its role in particle transport

Simultaneous with the formation of an edge temperature pedestal at the L-I transition, edge turbulence typically increases at frequencies > 150 kHz. This 'weakly coherent mode' (WCM) is evident at 240 kHz in the example of Figure 3.4-1. It is also detected in magnetic fluctuations measured on poloidal field pickup coils mounted outboard of the plasma on the low field side, and on Electron Cyclotron Emission (ECE) fluctuations [White 2011].

The WCM density fluctuations are also observed by Gas Puff Imaging (GPI) [Cziegler 2010]. The reflectometer, ECE and GPI measurements all show that the WCM is localized to the region of the strong edge temperature gradient. GPI measurements resolve the poloidal wavenumber, giving $k_\perp \rho_S \sim 0.1$, $n_{toroidal} \sim 20$ and show that the mode propagates in the electron diamagnetic direction in the plasma frame. An example is shown in Figure 3.4-2 [Hubbard 2011]. Detailed analysis of the ECE data shows that this signal is dominated by temperature fluctuations, with $\delta T_e/T_e \sim 2\%$ [White 2011]. This compares with a typical density fluctuation level, from GPI, of about 10%. This could be consistent with the WCM causing more particle than energy transport, perhaps being the main mechanism responsible for the edge particle transport (relative to that in H-mode) during I-mode operation.

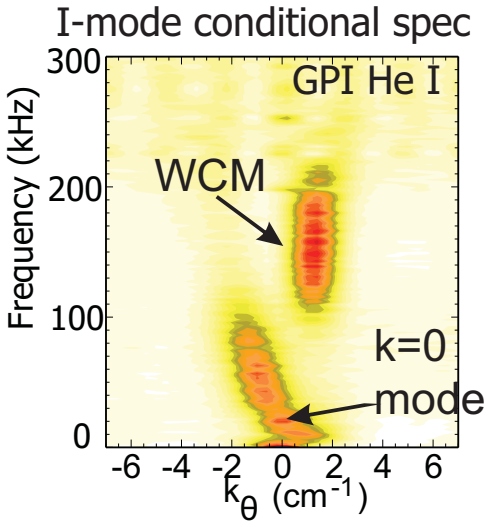

Figure 3.4-2: Conditional spectra of emissivity fluctuations measured by Gas Puff Imaging. The WCM feature is clearly visible, while a k=0 mode is difficult to see in the turbulence.

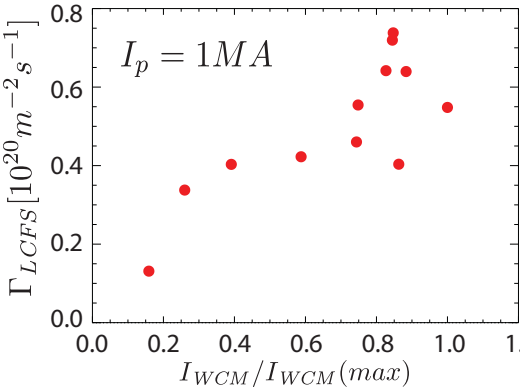

Figure 3.4-3: Particle flux as a function of the Weakly Coherent Mode (WCM) amplitude, for an I-mode experiment with I_p=1 MA and varied input power. From [Dominguez 2012].

As a test of this hypothesis, a series of experiments was performed to examine directly the relationship between density transport and the intensity of the WCM. The WCM amplitude was monitored using multiple frequencies of the reflectometry diagnostic and the deuterium particle source using an analysis of absolutely calibrated D_α imaging near the outboard midplane. Correlations were found between the radial particle flux Γ and the WCM amplitude, with an example shown in Figure 3.4-3 [Dominguez 2012]. This supports the conjecture that there is a causal relationship between the WCM and particle transport, analogous to that established by a similar technique between the QC mode and particle transport in EDA H-modes [Terry 2005].

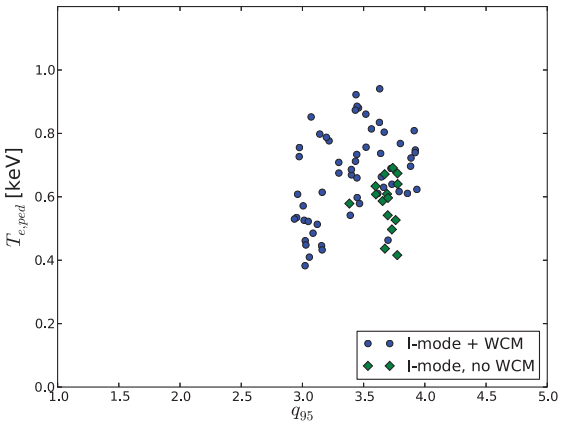

Figure 3.4-4: C-Mod I-modes with (blue) and without (green) weakly coherent mode. The discharges without WCM are at q_{95}>3.5 and moderate T_{ped}

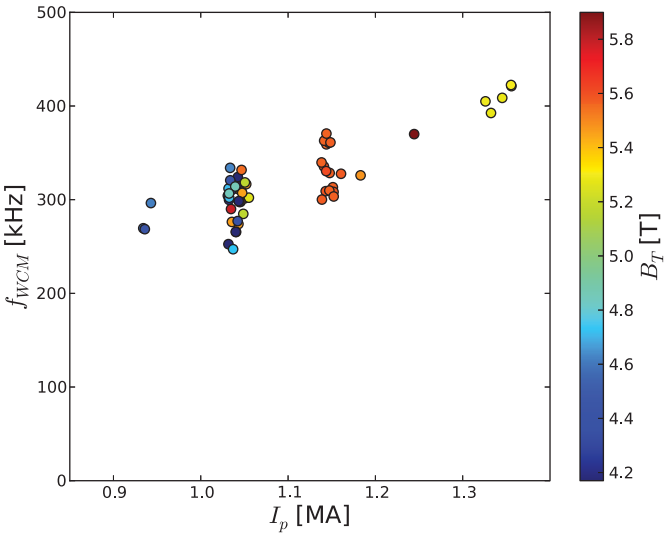

Figure 3.4-5: Center frequency of WCM, increasing with plasma current.

The WCM is strongest and most coherent in high temperature and performance I-modes, particularly at low q_{95}. It is thus very compatible with low collisionality. In some I-modes, particularly those with q_{95} >3.5 and/or input power which is marginal with respect to the L-I threshold, it is not distinguishable with available diagnostics, even though there is clear formation of a modest temperature pedestal. A number of examples of this were observed in the 2012 run campaign; in some cases phases with a WCM, and generally higher pedestals, follow phases with no WCM. The phases without WCM have some similarities to the I-modes observed in initial experiments on DIII-D, discussed in Chapter 4 of this Joint Research Target report.

If the edge is cooled, by reduction in net power, the WCM amplitude and frequency reduce and a transition to either L-mode or H-mode can result. An initial assessment of the pedestal database confirms that low q_{95} and high T_{ped} favor the WCM (Figure 3.4-4). The frequency of the mode varies with current or q_{95} (Figure 3.4-5), perhaps related to trends in pedestal rotation. While the physical mechanism of the mode is not yet clear, these observations suggest it may be driven by the strong edge temperature gradient characteristic of I-mode, or dependent on ν*. One candidate which has been proposed is the Heavy Particle Mode [Coppi 2012]. Identifying the mechanism of the mode is a key goal of the collaborative effort on gyrokinetic simulation discussed in Section 3.2, as well as these ongoing experimental studies.

4.3: Observations of GAM in I-mode

An exciting new observation in C-Mod I-modes is that of a fluctuating zonal flow in the edge region. This was detected using the same Gas Puff Imaging diagnostic previously used to measure the mode spectrum of the WCM. Velocimetry based on a time-delay-estimation (TDE) method has been recently implemented for use on the fast 2D array. This reveals a clear peak in poloidal velocity v_θ, fluctuations at typically 20 kHz, only during I-modes. An example, from the recent publication of Istvan Cziegler (UCSD Center for Momentum Transport and Flow Organization) [Cziegler 2013], is shown in Figure 3.4-6. Analysis of a number of discharges shows that its frequency scales with cs/(2pR), consistent with expectations and observations elsewhere of a Geodesic Acoustic Mode or GAM (Figure 3.4-7). This, along with analysis of its phase and coherence, identify it as a GAM.

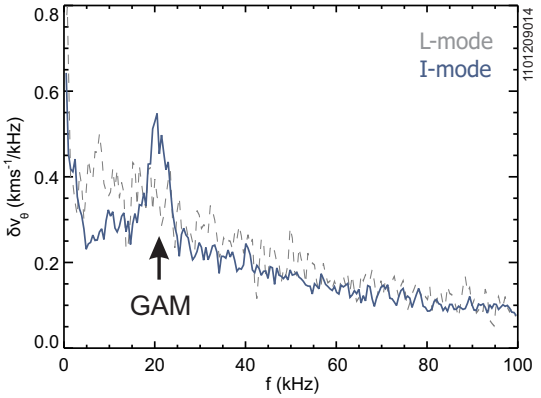

Figure 3.4-6: Poloidally averaged Fourier spectra of TDE poloidal velocities in an I-mode (solid blue) and the preceding L-mode (dashed grey). The sample size for correlation measurements is n_{cor} = 20. Spectra are time averaged from a spectrogram with df =0.5 kHz. [Cziegler 2013].

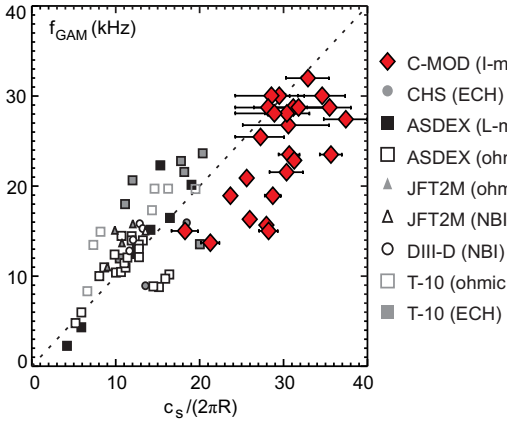

Figure 3.4-7: GAM frequencies against the theoretical c_s=R from a large number of experiments [Fujisawa 2007], with the recent results from Alcator C-Mod overlaid as the red squares. The dashed line represents $\omega = c_s/R$ [Cziegler 2013].

The observation is significant since GAMs have not previously been seen in any L-Mode or H-mode pedestals on C-Mod. In contrast, the GAM is seen in all I-mode discharges for which GPI data are available and which have been examined to date. It is not simply a transient phenomenon, but persists throughout the entire duration of the I-mode. An example is shown in Figure 3.4-8. Analysis indicates that a shift in the relative drive and damping terms for energy transfer to the GAM and the mean shear flow may be important in the I-H mode transition. This work, and similar analysis of L-H transitions, is being pursued by researchers at the Center for Momentum Transport and Flow Organization.

The GAM coexists with the previously observed WCM, which has much higher frequency, and appears to interact with it. Both modes exist in the same region, where the I-mode temperature pedestal is strong. Nonlinear spectral analysis indicates that energy is transferred between the WCM and the GAM; the fluctuating flow may well be responsible for the broad frequency of the Weakly Coherent Mode, which has been puzzling given its narrow poloidal wavenumber.

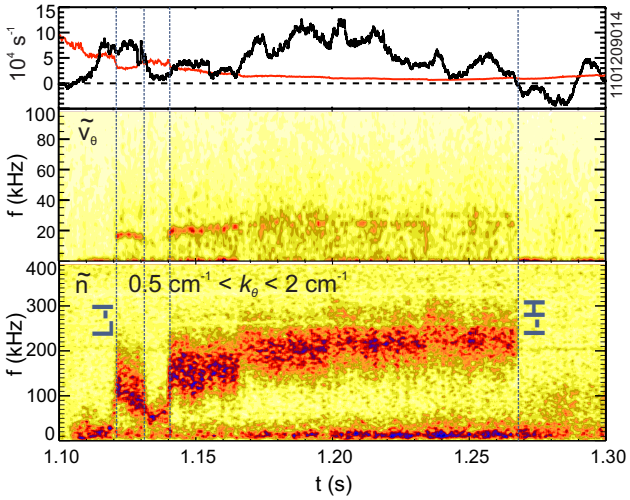

Figure 3.4-8: Evolution of the GAM (middle panel) and higher frequency Weakly Coherent Mode (lower panel), during an I-mode on Alcator C-Mod. In the top panel, the solid black line represents the estimated, time-resolved, non-linear GAM drive, and the red curve corresponds to 4νii/7q, related to the collisional damping rate; The I-H transition occurs when the drive drops below the damping. From [Cziegler 2013].

4.4: Changes in core turbulence at L-I transition

The reduction in broadband turbulence in the pedestal regions is, as was described in Section 4.1, one of the fundamental features of L-I transitions, and correlated to the decrease in edge thermal transport. A new and interesting observation is that core turbulence also drops significantly, and promptly, at the transition. An example is shown in Figure 3.4-9. The top contour plot shows a fluctuation spectrogram from a reflectometer channel at ρ=0.55, well inboard of the pedestal. These show a clear decrease at the L-I transition, across a broad range from 20 KHz to about 400 kHz. Because density does not change, in contrast to H-mode transitions, the reflection location stays nearly constant. No weakly coherent mode is seen in the core; as noted it is localized to the pedestal region.

More details of the time evolution and radial location of the turbulence changes are shown in Figure 3.4-10. The decrease at ρ =0.55 begins at the time that $T_{e,95}$ steps up at 0.87 s, the first dashed line. As frequently occurs, this step coincides with a sawtooth heat pulse. The slower decay of this pulse indicates a decrease in edge thermal transport, and the beginning of the L-I transition. The fluctuations at this pedestal location decrease at the same time, and to a similar degree, as those in the core. In contrast, the fluctuations at the extreme edge (ρ=0.99) do not decrease until t=0.891 s, the second dashed line. The Weakly Coherent Mode (not shown), does not appear until this later time. These

observations suggest that the trigger for the transition may be at or inboard of the pedestal, with the WCM onset triggered by the formation of the temperature pedestal.

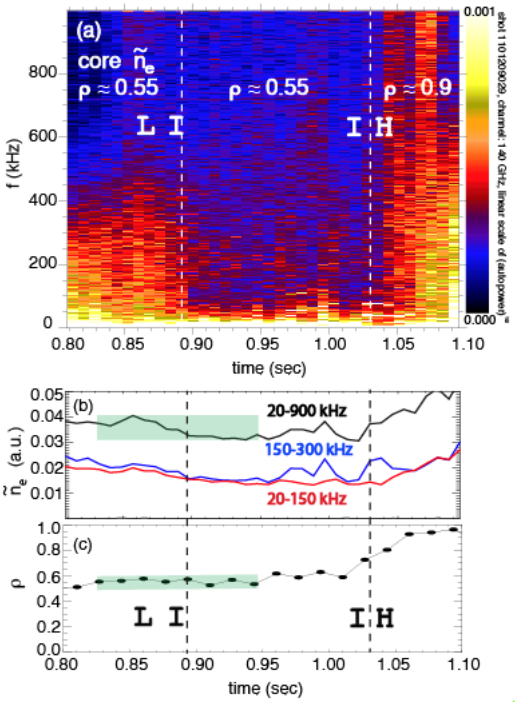

Figure 3.4-9: (a) Spectrogram of core density fluctuations across L-I transition and I-H transition. (b) Evolution of core density fluctuation level in different frequency ranges across the L-I transition. (c) Reflectometer radial measurement location remains fixed in time across the L-I transition. Green shaded region indicates time range of steady density across L-I transition.

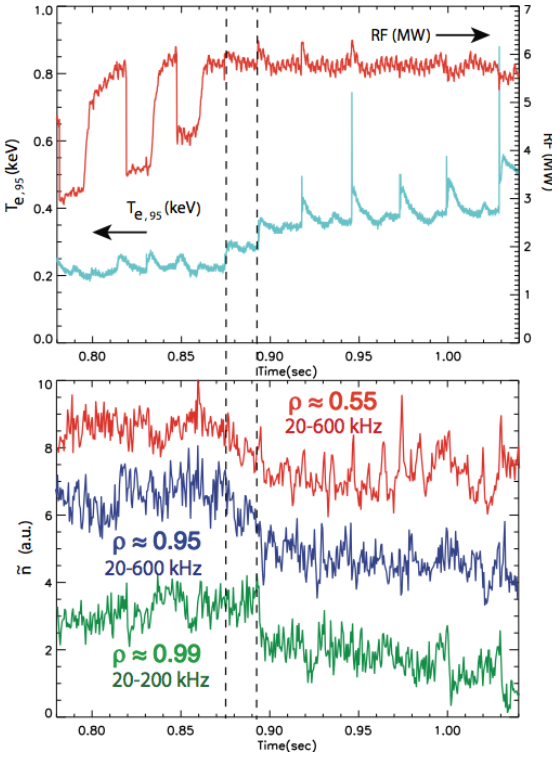

Figure 3.4-10: Temporal evolution of core and edge density fluctuation levels across the L-I transition, showing that core turbulence is reduced prior to characteristic changes in edge (ρ = 0.99) fluctuations in I-mode, and concomitant with the T_e increase, and fluctuation decrease, at ρ=0.95. The onset of the WCM (t = 0.891 sec) follows the reduction in core and pedestal turbulence.

The decrease in core density turbulence is seen in a larger set of I-mode discharges, and over a wide radial range, as shown in Figure 3.4-11. The decrease is up to 30%, and extends at least to ρ=0.45. A reduction in temperature fluctuations, measured with correlation ECE [Sung 2013] , is also observed, as shown in Figure 3.4-12. These show a significant reduction into at least ρ=0.74, the furthest this diagnostic can currently view.

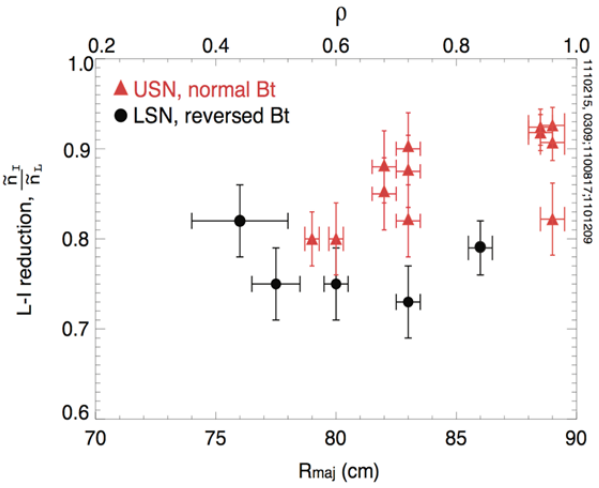

Figure 3.4-11: Relative change in density fluctuation amplitude, n-tilde, in I-mode compared to L-mode, n-tilde$_I$/n-tilde$_L$, is plotted versus radius. Since density is constant across the transition the reduction, measured with reflectometry, indicates that the relative fluctuation level n-tilde/n is reduced in I-mode.

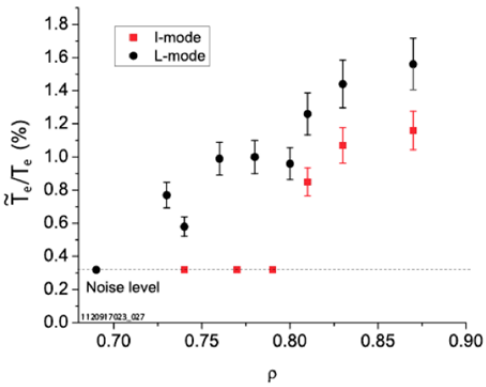

Figure 3.4-12: Reduction of long wavelength ($k_\theta \rho_s < 0.3$) broadband electron temperature fluctuation amplitude ($0 < f < 400$ kHz), in I-mode (red) compared to L-mode (black), is plotted versus radius.

The reduction in turbulence is consistent with the increase in electron and ion temperatures across the core profile in I-modes. An example of changes in core profiles is shown in Figure 3.4-13. Analysis of transport changes in terms of growth rates and ExB shearing rates is in progress. The growth rate is calculated using GYRO [Candy 2003], and in both L-mode and I-mode the fastest growing mode is identified as an Ion Temperature Gradient mode (ITG).

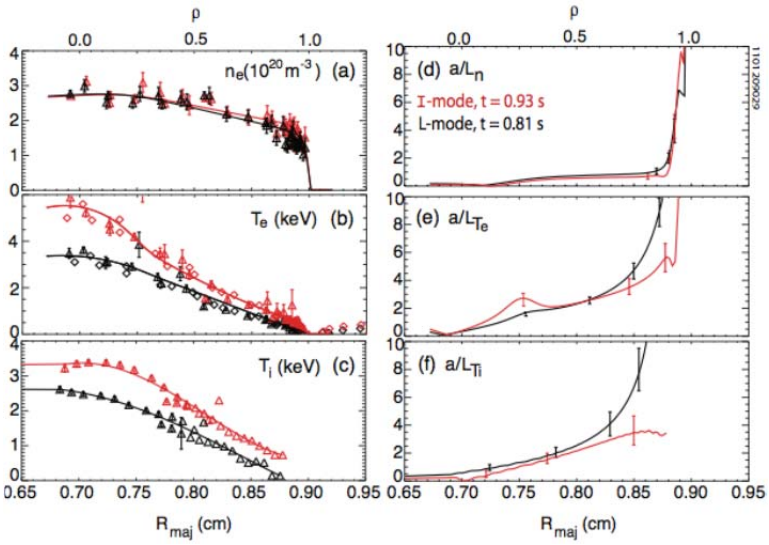

Figure 3.4-13: Changes in core density, electron temperature and ion temperature profiles across the L-I transition. I-mode profiles are in red, L-mode in black.

A paper describing these exciting new results on core turbulence and transport changes in I-mode will soon be submitted for publication by Anne White, Choongki Sung and colleagues [White 2013].

5.0 Remaining issues and opportunities for further work.

Much progress has been made during FY13 in the analysis and understanding of the I-mode regime on Alcator C-Mod. The regime remains highly attractive for fusion reactor scenarios, due to its combination of high energy confinement and low particle confinement. It has been demonstrated to operate at the ITER q_{95} with high performance, and shows high confinement at ITER-relevant low collisionality and external torque. There are no known physics barriers to extrapolate the I-mode regime to burning plasmas. However, further work is required to confidently extrapolate the regime to ITER, and to fully understand the physics of the regime. Many opportunities to advance this promising research remain. Some will require new experiments on Alcator C-Mod, others could be accomplished by further analysis of existing data, following up on the results recently obtained. Comparisons with I-mode experiments on other tokamaks, including those on DIII-D (see Chapter 4) and with ASDEX Upgrade and potentially several other international devices as part of ITPA joint activities will also be valuable.

In the area of expansion of operating space, the key issues are to reliably increase the input power without an I-H transition, to increase the plasma density towards higher Greenwald fraction, and to demonstrate high normalized pressure β as well as high absolute pressure. The initial experiments with fueling into an I-mode revealed a promising path for further optimization. Experiments at reduced B_T (2.6-3.5 T) would be helpful to assess whether there is a physics limit to pedestal β, since at 5 T or higher the maximum pressure and power have been limited by the available heating. Further investigation of shaping and divertor configuration would also be valuable to understand the surprising differences between operating spaces for upper and lower null plasmas illustrated in Figure 3.2-3.

Further experiments are also needed for a full characterization and analysis of the turbulence and transport which are fundamental to the I-mode regime. The observations of GAMs with GPI, which were not extracted from the data until after the last campaign, strongly motivate measurements over a wider range of parameters to understand the role of these fluctuating flows. More measurements of mean flows and E_r will also be valuable. Because both GPI and CXRS require special gas puffing these measurements are not available from the majority of prior experiments. Further information on the Weakly Coherent Mode, and potentially the GAMs, could be obtained with specialized scanning probe diagnostics, such as a magnetic probe head to measure fluctuations in B and the newly developed Mirror Probe. Important questions remain about the exact radial location and extent of these fluctuations with respect to the E_r well. Finally, use of the active 'Shoelace antenna' which was demonstrated during the FY12 campaign to

interact with quasicoherent modes in EDA H-mode plasmas, and which has been upgraded during the recent maintenance period, provides an exciting opportunity to actively control pedestal particle transport and perhaps extend the I-mode regime. In the area of core turbulence and transport, the CECE diagnostic has been upgraded to probe T_e fluctuations further into the plasma. Measurements of both temperature and density fluctuations are currently limited to a small number of discharges and could be greatly extended.

Many opportunities also remain for analysis and interpretation of existing data. Techniques for analysis and interpretation of CXRS with the gas puff technique, including deconvolution of instrumental effects, have only recently been optimized. We can now apply these to a range of I-modes and investigate with more confidence the details of flows, T_i and E_r, scalings with plasma parameters, and the surprising differences in potential and/or ion temperature observed between high and low field side measurements. Stability analysis of the I-mode pedestal should be extended to other cases, including the less typical examples which did have some ELMs, to understand the limiting modes. Much remains to be done in the microstability analysis of I-mode, which has the potential to reveal the physical mechanisms of the Weakly Coherent Mode. We also hope to collaborate with theorists, including groups at UC San Diego, Univ. Wisconsin and elsewhere. The ultimate goal of this research is to understand the physics which leads to the surprising, but highly beneficial, separation of thermal and particle transport. Only with this understanding can we confidently extrapolate the I-mode regime to other experiments, including ITER and future reactors.

References

[Candy 2003] Candy J. and Waltz R.E., *J Comput. Phys.* **186**, 545 (2003).
[Carlstrom 1998] T.N. Carlstrom, K. H. Burrell and R. J. Groebner, Plasma Phys. Control. Fusion **40** 669 (1998).
[Churchill 2013a] R.M. Churchill *et al*, Rev. Sci. Instrum. **84** (2013) 0935005.
[Churchill 2013b] R.M. Churchill, B. Lipschultz, C. Theiler, and the Alcator C-Mod team, *In-Out Impurity Density Asymmetry in the Pedestal Region of Alcator C-Mod*, submitted for publication.
[Coppi 2012] B. Coppi and T. Zhou, Physics of Plasmas **19**, (2012) 012302.
[Connor 1979] J.W. Connor and R.J. Hastie, Proc. Royal Soc. London (1979).
[Cziegler 2010] I. Cziegler, *et al*, Physics of Plasmas, **17**(2010) 056120.
[Cziegler 2013] I. Cziegler, P. H. Diamond, N. Fedorczak, P. Manz, G. R. Tynan, M. Xu, A. E. Hubbard, B. Lipschultz, J. M. Sierchio, J. L. Terry, and C. Theiler, Physics of Plasmas **20** 055904 (2013).
[Dominguez 2012] A. Dominguez, Ph.D. Thesis, Physics Department, Massachusetts Institute of Technology (2012).
[Dudson 2009] B.D Dudson, *et al*. Comput. Phys. Commun. **180** (2009) 1467.
[Fujisawa 2007] A. Fujisawa, *et al*., Nucl. Fusion **47**, S718 (2007).
[Greenwald 1997] M. Greenwald, R.L. Boivin, F. Bombarda, P.T. Bonoli, C.L. Fiore, D. Garnier, J.A. Goetz, S.N. Golovato, M.A. Graf, R.S. Granetz *et al*, Nuclear Fusion **37** (6), 793 (1997).
[Greenwald 1999] M. Greenwald, R. Boivin, P. Bonoli, R. Budny, C. Fiore, J. Goetz , R. Granetz, A. Hubbard, I. Hutchinson, J. Irby *et al*, Physics of Plasmas **6**(5) 1943-9 (1999).
[Groebner 1998] R. J. Groebner and T.N. Carlstrom, Plasma Phys. Control. Fusion **40** 673 (1998).
[Groebner 2013] R.J. Groebner, C.S. Chan, J.W. Hughes, R. Maingi, P.B. Snyder *et al*, Nucl. Fusion **53** (2013) 093024.
[Howard 2011] N.T. Howard, *et al*, Review of Scientific Instruments, **82** (2011) 033512.
[Hubbard 2007] A. E. Hubbard. J. W. Hughes, I. O. Bespamyatnov, T. Biewer, I. Cziegler, B. LaBombard, Y. Lin, R. McDermott, J. E. Rice, W. L. Rowan, J. A. Snipes, J. L. Terry, S. M. Wolfe, S. Wukitch and the Alcator C-Mod Group, Phys. Plasmas **14** (5) 056109 (2007).
[Hubbard 2011] A.E. Hubbard, *et al*, Phys. Plasmas **18** (2011) 056115.
[Hubbard 2012] A E Hubbard, D G Whyte, R M Churchill, A Dominguez, J W Hughes, Y Ma, E S Marmar, Y Lin, M L Reinke and A E White, Nucl. Fusion **52** (2012) 114009.
[Hughes 2013] J.W. Hughes, P.B. Snyder, J.R. Walk, *et al*, Nuclear Fusion **53** 043016 (2013).
[ITER 1999] ITER Physics Expert Groups on Confinement and Transport and Confinement Modelling and Database, *et al*, Nucl. Fusion **39** (1999) 2175.

[Martin 2008] Y. Martin, T. Takizuka and ITPA CDBM H-mode Threshold Database Working Group *J. Physics: Conf Series*. **123** 012033 (2008).
[McDermott 2009] R. McDermott *et al* Phys. Plasmas **16** 056103 (2009).
[Mossessian 2003] D.A. Mossessian *et al*, Phys. Plasmas **10** (2003) 1720.
[Rice 2011] J.E. Rice, J.W. Hughes, P.H. Diamond, *et al*, Phys. Rev. Lett. **106**, 215001 (2011).
[Ryter 1998] F. Ryter, W. Suttrop, B. Brusehaber, M. Kaufmann, V. Mertens, H. Murmann, A. G. Peeters, J. Stober, J. Schweinzer, H. Zohm and ASDEX Upgrade Team, Plasma Phys. Control. Fusion **40**, 725-729 (1998).
[Sung 2013] C. Sung, A. E. White, N. T. Howard, *et al*, Nucl. Fusion **53** (2013) 083010.
[Snyder 2009] P.B Snyder, R.J. Groebner, A.W. Leonard, T.H. Osborne and H.R. Wilson *Phys. Plasmas* **16** 056118 (2009).
[Synder 2012] P.B. Snyder, *et al*. Nucl. Fusion **51** (2011) 103016.
[Terry 2005] J. L Terry, *et al*, Nuclear Fusion **45** (2005)1321.
[Walk 2012] J. R. Walk, P. B. Snyder, J. W. Hughes, J. L. Terry, A. E. Hubbard and P. E. Phillips, Nucl. Fusion. **52** (2012) 063011.
[White 2011] A. E. White, P. Phillips, D. G. Whyte, A. E. Hubbard, C. Sung, J. W. Hughes, A. Dominguez, J. Terry and I. Cziegler, Nucl. Fusion **51** 113005 (2011).
[White 2013] A. E. White, *et al*, *Reduction of Core Turbulence in I-mode Plasmas in Alcator C-Mod* to be submitted to Nuclear Fusion.
[Wilson 2002] H.R.Wilson*, et al*. Phys. Plasmas **9** (2002) 1277.
[Whyte 2010] D. G. Whyte, *et al*, Nuclear Fusion **50** 105005 (2010).